

## **Three-Terminal III-V/Si Tandem Solar Cells Enabled by a Transparent Conductive Adhesive**

Manuel Schnabel,<sup>\*a</sup> Henning Schulte-Huxel,<sup>a,b</sup> Michael Rienäcker,<sup>b</sup> Emily L. Warren,<sup>a</sup> Paul F. Ndione,<sup>a</sup> Bill Nemeth,<sup>a</sup> Talysa R. Klein,<sup>a</sup> Maikel F.A.M. van Hest,<sup>a</sup> John F. Geisz,<sup>a</sup> Robby Peibst,<sup>b</sup> Paul Stradins,<sup>a</sup> Adele C. Tamboli<sup>a</sup>

<sup>a</sup>National Renewable Energy Laboratory, Golden CO 80401, USA

<sup>b</sup>Institute for Solar Energy Research Hamelin, D-31860 Emmerthal, Germany

### **SUPPORTING INFORMATION**

This file includes supporting information on the following four topics:

1. ITO optimization – Optics (including details on raytracing simulations)
2. ITO validation – contact resistance and recombination
3. Solar Cell Efficiency Measurement
4. Solar Cell Current-Voltage Fitting

Each topic starts on a new page. A list of references is provided on the last page.

## 1. ITO optimization - Optics

To achieve optimized performance, we varied the sputtering power and substrate temperature during the deposition of sputtered indium tin oxide (ITO). The complex refractive indices ( $n&k$ ) of the resulting films on glass were obtained by fitting ellipsometry data measured with a J. Woollam M-2000 ellipsometer using WVASE software (see Fig. S1), and were then fed into a raytracing simulation of the entire three-terminal GaInP/Si tandem cell using the PVLighthouse SunSolve™ calculator<sup>1</sup> to calculate the expected short-circuit current density ( $J_{sc}$ ) of the Si sub-cell for the different ITO recipes.

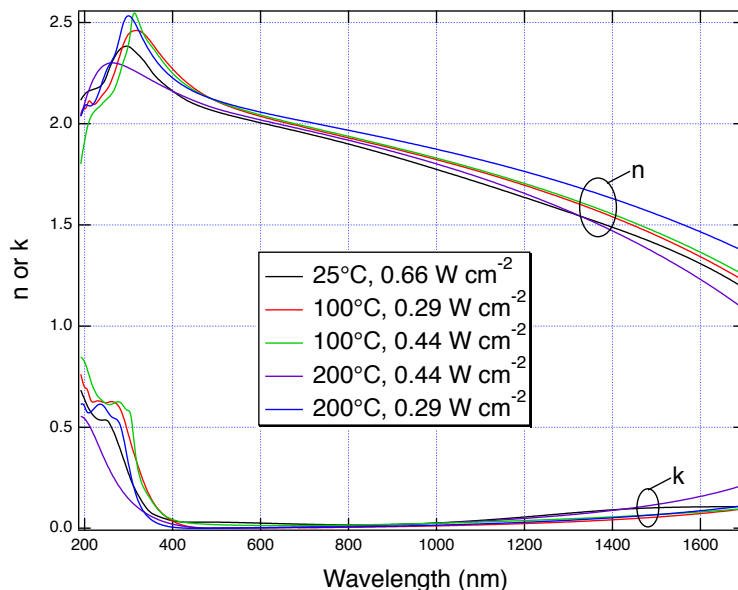


Figure S1. Complex refractive indices ( $n&k$ ) for different ITO recipes determined by ellipsometry.

The SunSolve™ calculator from PVLighthouse<sup>1</sup> was selected because its raytracing algorithm is suited to silicon wafers, and because it is easy to use and publicly available. The structure used to simulate the actual three-terminal tandem (3TT) cell presented in the main manuscript is shown below (Fig. S2). Many complex refractive index datasets are available on the PVLighthouse website; the proprietary ones are labelled “custom” in the figure below and were measured on films that are nominally identical to the ones implemented in the 3TT GaInP/Si tandem cell. The default Lambertian scattering fraction of 0.5 was used for the rear side of the Si wafer.

The grid dimensions in the active cell area were determined using photolithography mask dimensions for the length of fingers and busbars, and microscope images for the widths. The result is a grid with 2.6% coverage, which was also implemented in the simulation (the only difference being that the tapered busbar was implemented as one with uniform width and equal area). The microspheres of the transparent conducting adhesive (TCA) are not implemented in the simulation. However, it is known from prior studies that each area percent of microspheres in the TCA leads to 1% loss in transmission.<sup>2</sup> We therefore reduce the Si  $J_{sc}$  predicted by the simulation by the area percent coverage of microspheres (3.1%) in the final cell before reporting it in Table 1 of the main manuscript and Table S1 (below). When texture is added to the simulation, random pyramids of default dimensions are added.

The SunSolve™ simulations were used to optimize the thickness of the two ITO layers (above and below the TCA) to within 5 nm for each ITO recipe. The results are shown in Table S1 (reproduced from Table 1 of the main manuscript), along with the value calculated for a structure without index-grading ITO layers.

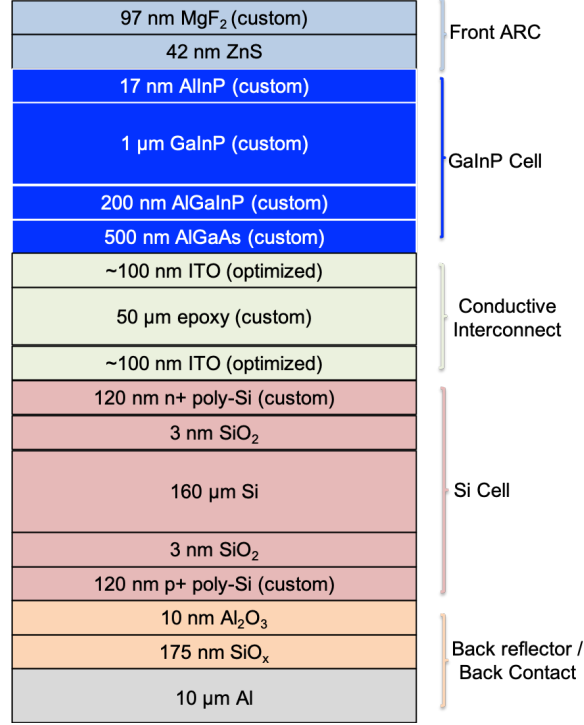


Figure S2. Layer structure used to perform optical simulations of the 3TT cell using Sunsolve™.

Table S1: Simulated  $J_{sc}$  of the Si bottom cell in a GaInP/Si 3TT cell for different ITO recipes at optimized thicknesses of the ITO above the TCA ( $d_{ITO,top}$ ) and below the TCA ( $d_{ITO,bot}$ ). The simulated  $J_{sc}$  without ITO layers is also shown.

Substrate Temperature (°C)	Sputter Power (W cm <sup>-2</sup> )	$J_{sc}$ (mA cm <sup>-2</sup> )	$d_{ITO,top}$ (nm)	$d_{ITO,bot}$ (nm)
-	-	16.2	0	0
25	0.66	17.9	90	85
100	0.29	18.9	95	95
100	0.44	18.3	95	95
200	0.29	19.0	95	95
200	0.44	18.3	95	90

To determine whether the improved Si  $J_{sc}$  is due to differences in the extinction coefficient  $k$  or the refractive index  $n$  of the ITO, the simulations were repeated with the extinction coefficient set to zero for all ITO films. From best to worst the five ITO recipes remain in the same order, but the difference between the 25°C, 0.66 W cm<sup>-2</sup> and the 200°C, 0.29 W cm<sup>-2</sup> recipe shrinks from 1.1 to 0.5 mA cm<sup>-2</sup>. This shows that both  $n$  and  $k$  need to be optimized for good light coupling to the Si bottom cell.

The optimum refractive index of an antireflection coating (ARC) is the geometric mean of the refractive indices of the media it is between ( $n = (n_{above}n_{below})^{1/2}$ ), which, averaging across the relevant wavelength range for a Si cell below GaInP (650 nm-1200 nm), yields 2.23 for an ARC between AlGaAs and TCA, and 2.35 for an ARC between TCA and n+ poly-Si (the 25°C, 0.66 W cm<sup>-2</sup> and 200°C, 0.29 W cm<sup>-2</sup> recipes have averaged refractive indices of 1.85 and 1.93, respectively). However, for Sunsolve™ simulations with idealized ARCs at these locations in the cell stack a wavelength-dependent idealized refractive index was used, i.e.  $n(\lambda) = (n_{above}(\lambda)n_{below}(\lambda))^{1/2}$ , where  $\lambda$  is the wavelength.

## 2. ITO validation – contact resistance and recombination

Having found a reasonably optimized ITO recipe (200°C, 0.29 Wcm<sup>-2</sup>) for optical coupling to the Si bottom cell, we proceeded to verify that sputtered ITO makes good contact to the two sub-cells and that the sputtering process does not damage the sub-cells.<sup>3</sup> To measure contact resistance of the ITO to p<sup>+</sup> AlGaAs (bottom layer of the GaInP cell) and n<sup>+</sup> poly-Si (top layer of the Si cell) ITO was sputtered onto these layers. A transmission line (TLM) pattern<sup>4</sup> of 4 nm Ti / 1 μm Ag contacts was evaporated onto the ITO using a shadow mask, and the ITO removed between the contacts by etching in dilute HF. Contact resistances below 10 mΩ cm<sup>2</sup> were obtained in both cases, which is more than sufficient for one-sun applications.

To assess the effect of sputter damage on the GaInP cell, multiple GaInP cells were grown as described in the Methods section of the main manuscript, and some had ITO sputtered on them (100°C, 0.29 W cm<sup>-2</sup>). The ITO was removed in dilute HF, and all GaInP cells were processed onto dummy Si substrates for characterization.<sup>5</sup> The efficiency of GaInP cells exposed to ITO was 0.7%(relative) lower, which is insignificant compared to a standard deviation in efficiency of identical devices of 2.6%(relative). Similarly, the impact of ITO deposition on the 3T Si cells was determined, in this case via quantitative analysis of photoluminescence images taken before and after ITO deposition, which yields an implied difference in  $V_{oc}$ ,<sup>6</sup> the main parameter affected by sputter damage.<sup>3</sup> A  $V_{oc}$  loss of 1 mV was obtained, which is negligible (<0.2%), and shows that sputtered ITO can be used as a conductive index-grading layer without impacting the electrical performance of the sub-cells.

### 3. Solar Cell Efficiency Measurement

RSC journals have guidelines shown below (in bold) for reporting efficiencies. The way we address them is given in plain text.

**A full, conventional error analysis should be carried out and reported. This should consist of both random and systematic/bias analyses of values to support the main claims presented in the article, and information on how the error analysis was carried out.**

To estimate the errors in our solar cell measurements, we conferred with NREL's certification laboratory to obtain the errors that they would apply. We then increase them based on shortcomings of our setup relative to the certification laboratory, as detailed in the following.

Open-circuit voltage ( $V_{oc}$ ): The certification laboratory error is 1.0%. However,  $V_{oc}$  depends on temperature, and the "instantaneous"  $V_{oc}$  approach that we use to set temperature, detailed below, also has an error. We estimate an additional random error of 0.5% of  $V_{oc}$  and deduce an overall error of 1.5%.

Short-circuit current density ( $J_{sc}$ ): The certification laboratory error is 1.3%. The additional error in irradiance arising from fluctuations in the lamp current between setting up the illumination and completing measurements is estimated to be 1%, based on reference cell measurements before and after the cell measurement, and on prior knowledge of how observed fluctuations in the lamp current affect irradiance. The error arising from the different heights of the reference cell and device under test, which is corrected for by manually adjusting the height of the stage, is estimated at another 1%, based on prior experience of the variation of irradiance with stage height. This gives an overall error of 3.3%.

Fill Factor ( $FF$ ): The certification laboratory error is 0.6%. Since  $FF = J_{mpp}V_{mpp}/J_{sc}V_{oc}$ , where subscript mpp refers to the value at maximum power point, we consider potential additional errors in  $V_{mpp}/V_{oc}$  and  $J_{mpp}/J_{sc}$ . We do not expect a meaningful additional error in the former, and while  $J_{mpp}/J_{sc}$  is also affected by fluctuations in lamp intensity, an IV curve is swept quickly enough that this error too is minimal. We therefore also apply an error of 0.6%.

Since  $V_{oc}$ ,  $J_{sc}$ , and  $FF$  are multiplied to give the efficiency, we sum the squares of the relative errors and square-root the result to obtain an RMS efficiency error of 3.7% relative, or about 1% absolute for the two-terminal tandem (2TT) and three-terminal tandem (3TT) efficiencies.

However, we also report an efficiency *difference* between the 2TT and 3TT tandem cell efficiency. When calculating a difference, systematic errors in the original values cancel out, and only the random error needs to be applied. The random error is estimated by looking at the range of values obtained upon repeated measurement. Specifically, we quantify the relative random error as (maximum-minimum)/average for the efficiencies measured in the 2TT, GaInP, and Si IBC circuits (see Table 2 of the main manuscript), before and after the 3TT measurement, which yields 0.4% relative. We apply this relative error to the 2TT, 3TT FB, and 3TT IBC efficiencies, and sum the resulting absolute errors to yield 0.2% absolute. This is the error with which the efficiency improvement upon going from 2TT to 3TT operation is reported.

**Efficiencies should be reported to an appropriate number of significant figures, along with a standard deviation.**

As described above, the error in the absolute efficiencies is 3.7% relative, so we report efficiencies to 3 significant figures. Similarly,  $FF$  and  $J_{sc}$  are reported to 3 significant figures.  $V_{oc}$  is reported to the nearest mV because that is common practice. Only one cell of each type was available, so a standard deviation from multiple devices cannot be provided.

**A sufficient number of samples should be tested, and a sufficient number of trials performed.**

Only one three-terminal (3TT) cell and one comparable four-terminal (4TT) reference device were available. Illuminated current-voltage (light IV, LIV) curves were measured at least three times in succession. The standard deviation in efficiency is 0.2% relative, mainly arising from  $J_{sc}$ .

**The 1 Sun AM 1.5G reference spectrum should be used as standard for testing power conversion efficiency.**

AM1.5G was used as the target incident spectrum, and the illumination from a filtered Xe lamp and three infrared (780 nm, 810 nm, 940 nm) LEDs was adjusted such that, corrected for spectral mismatch, both sub-cells saw one-sun AM1.5G conditions. Experimentally measured external quantum efficiency curves were used to calculate the spectral mismatch factor required for the correction.

**Full experimental conditions under which the efficiency is measured should be declared.**

The active area of the 3TT device, set by a shadow mask, was measured with a light microscope to be  $0.567 \pm 0.001 \text{ cm}^2$ . It included the grid and the busbar on the top of the cell but did not include busbars on the bottom of the cell. The shadow mask was made of black cardboard which has negligible transmission at all wavelengths between 200-1500 nm (-0.03% to 0.02% were measured using a Cary 5000 spectrophotometer, which is at the resolution limit of the instrument).

One-sun AM1.5G conditions were set by adjusting the height of a filtered Xe lamp such that the irradiance of the GaInP sub-cell, corrected for spectral mismatch, is one sun. A  $25\text{mm}^2$  GaInP reference cell with certified one-sun performance was used. Then, infrared LED illumination was added to the incident spectrum such that the irradiance of the Si sub-cell, corrected for spectral mismatch, is also one sun. The incident spectrum was measured with a spectrophotometer to ensure the accuracy of the spectral mismatch correction. Three different infrared LEDs, emitting at 780 nm, 810 nm, and 940 nm, were used to improve spatial homogeneity of the LED illumination. Both a GaInP-filtered Si reference cell which is larger than the cell to be measured, and a 1.03 eV GaInAs reference cell which is smaller than the cell to be measured, indicated that 0.992-1.004 suns illumination had been obtained for the Si sub-cell, suggesting that any systematic error arising from spatially inhomogeneous illumination is negligible.

The measurement was performed at an effective cell temperature of  $25^\circ\text{C}$ . To maintain  $25^\circ\text{C}$ , the cell is allowed to equilibrate in the dark on a chuck maintained at  $25^\circ\text{C}$ . The cell's  $V_{oc}$  under instantaneous illumination is measured at a chuck temperature of  $25^\circ\text{C}$ , and the chuck cooled to a lower temperature ( $21.5^\circ\text{C}$  for the 3TT cell studied here) such that the cell maintains this  $V_{oc}$  under continuous illumination

(the  $V_{oc}$  is essentially used as the cell's own internal thermometer).<sup>7</sup> The measurement was performed in air, and no hysteresis was observed.

Measurement of the full 3TT performance (Fig. 5 in main manuscript) takes about 30 min. During this time, the irradiance cannot be monitored, but the lamp current was stable to within the accuracy of the power supply display (~0.25%) which we know from experience means the irradiance from the lamp is fluctuating by less than 1%. The illumination for both the GaInP and Si cells, as determined using primary calibrated reference cells, was 0.992-1.004 suns before and after the measurement.

**Independent certification of the photovoltaic performance of the device being reported is encouraged when the main claims rely on the absolute efficiency value being reported.**

The NREL certification laboratory is not currently able to certify devices where two source-meters must be addressed simultaneously, preventing certification of the full 3TT device. In order to present a self-consistent dataset we therefore report in-house measurements. However, we followed as many certification protocols as we could during our measurements, including spectral mismatch correction, correction for sample heating<sup>7</sup>, and accurate determination of the device area.

**If incident photon-to-current efficiency (IPCE), also referred to as external quantum efficiency (EQE) measurements are performed, the results should be integrated to a resulting short circuit current that can be compared with 1 Sun AM 1.5G power conversion efficiency data. The details of how this calculation is done and any correction factors should be clearly defined.**

EQE measurements were performed on a custom instrument and  $J_{sc}$  values are obtained by multiplying the EQE by the AM1.5G solar spectrum (in units of photons  $\text{cm}^{-2} \text{s}^{-1} \text{nm}^{-1}$ ), integrating over all wavelengths with finite EQE, and multiplying by the elementary charge to convert from electrons  $\text{cm}^{-2} \text{s}^{-1}$  to current density in  $\text{mA cm}^{-2}$ . The table below compares  $J_{sc}$  from EQE (see also Fig. 4(c) of main manuscript) to  $J_{sc}$  from our solar simulator (LIV, see Table 2 of main manuscript).

Table S2.  $J_{sc}$  values from LIV and EQE measurements of the 3TT cell and the 4TT reference device, in  $\text{mA cm}^{-2}$ . The LIV values correspond to those in Table 2 of the main manuscript, and the EQE values correspond to those in Fig. 4(c) of the main manuscript.

	3TT LIV	3TT EQE	4TT LIV	4TT EQE
$J_{sc, \text{GaInP}} (\text{mA cm}^{-2})$	14.8	14.5	14.9	15.1
$J_{sc, \text{Si}} (\text{mA cm}^{-2})$	19.9*	19.0	23.5	23.5

\*The Si sub-cell of the 3TT device could only be measured with the GaInP cell at open circuit, which leads to enhanced luminescent coupling and an artificially inflated  $J_{sc}$ .<sup>8</sup> A more appropriate value is obtained by summing  $J_{FB}$  and  $J_{IBC}$  at  $V_{FB}=V_{IBC}=0$  in Fig. 5 of the main manuscript, yielding  $19.2 \text{ mA cm}^{-2}$ .

It can be seen that the numbers agree very well, to within the aforementioned experimental error for  $J_{sc}$ . The only exception is the Si sub-cell of the 3TT device, but as noted above this is due to the GaInP cell inevitably being at  $V_{oc}$  during the Si IBC LIV measurement (with reference to Fig. 1(d) of the main manuscript it can be seen that there is no way to short-circuit or bias the GaInP cell without interfering with the Si IBC LIV measurement across contacts 2 and 3), and the value derived from Fig. 5 of the main manuscript,  $19.2 \text{ mA cm}^{-2}$ , is in rather good agreement with the  $19.0 \text{ mA cm}^{-2}$  from EQE.

## 4. Solar Cell Current-Voltage Fitting

The sub-cell LIV curves shown in Fig. 4(b) of the main manuscript were fitted to Eq. 1 of the main manuscript (single diode model), and implications of the fitting parameters were discussed in the main manuscript. Shown below in Fig. S3 are the fits to the four LIV curves performed using pvfit.<sup>9</sup> Fit parameters are tabulated in Table S3. It should be noted that each LIV curve was measured at least three times, each measurement was fitted, and all differences described in the manuscript exceed one standard deviation of the fit parameter (the latter is shown as an error in Table S3).

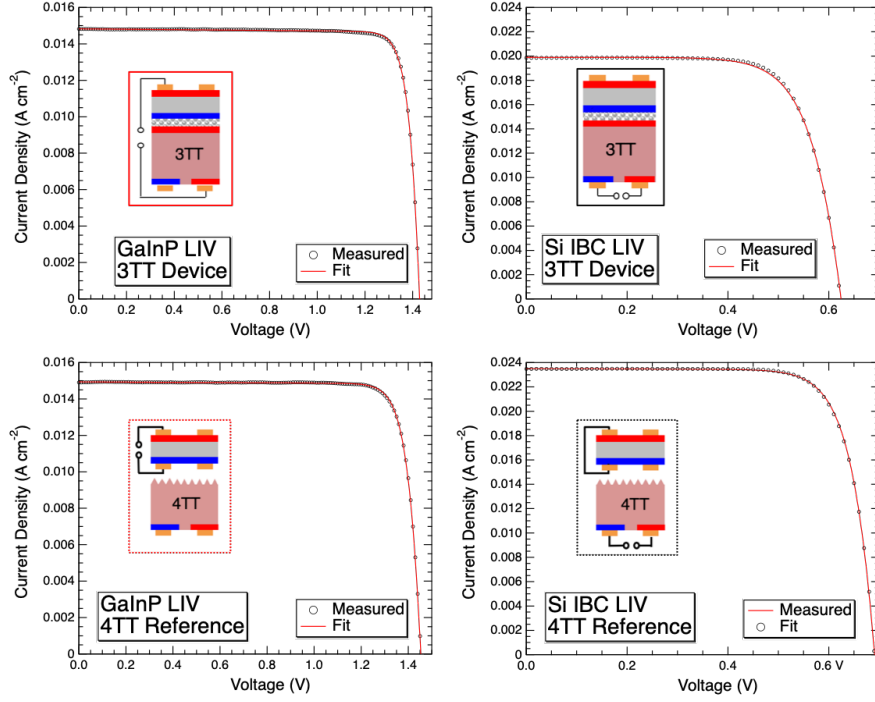


Figure S3. Fits of single-diode model (Eq. 1 in main manuscript) to the measured LIV curves in Fig. 4(b) of the main manuscript. Measurement circuits are shown as insets, and follow the color scheme of Fig. 1 in the main manuscript.

Table S3: Fitting parameters for the fits shown in Fig. S3. The following are tabulated: short-circuit current density  $J_{sc}$ , saturation current density  $J_0$  and ideality factor  $n$  of the diode, series resistance  $R_s$ , and shunt resistance  $R_{sh}$ . The errors given are the standard deviations derived from fits to at least 3 nominally identical LIV measurements for each cell/measurement. The fitting algorithm did not return a finite  $R_{sh}$  for any of the LIV curves measured on the Si IBC circuit of the 3TT device.

Measurement	GaInP LIV		Si IBC LIV	
	3TT	4TT ref.	3TT	4TT ref.
$J_{sc}$ ( $A\ cm^{-2}$ )	$0.01483 \pm 0.00003$	$0.01494 \pm 0.00002$	$0.01990 \pm 0.00002$	$0.023497 \pm 0.000006$
$J_0$ ( $A\ cm^{-2}$ )	$(4 \pm 0.8) \times 10^{-20}$	$(5.16 \pm 0.5) \times 10^{-17}$	$(5.89 \pm 0.08) \times 10^{-8}$	$(6.7 \pm 0.1) \times 10^{-10}$
$n$	$1.378 \pm 0.007$	$1.700 \pm 0.004$	$1.910 \pm 0.002$	$1.549 \pm 0.001$
$R_s$ ( $\Omega\ cm^2$ )	$0.64 \pm 0.02$	$0.91 \pm 0.01$	$0.576 \pm 0.006$	$0.2826 \pm 0.0007$
$R_{sh}$ ( $\Omega\ cm^2$ )	$9000 \pm 800$	$16000 \pm 800$	-	$11700 \pm 700$

## References

1. PVLighthouse, SunSolve™, <https://www.pvlighthouse.com.au/sunsolve>, (accessed 10.05.2018).
2. T. R. Klein, B. G. Lee, M. Schnabel, E. L. Warren, P. Stradins, A. C. Tamboli and M. F. A. M. van Hest, *ACS Applied Materials & Interfaces*, 2018, **10**, 8086-8091.
3. B. Demaurex, S. D. Wolf, A. Descoedres, Z. C. Holman and C. Ballif, *Applied Physics Letters*, 2012, **101**, 171604.
4. H. H. Berger, *Journal of the Electrochemical Society*, 1972, **119**, 507-514.
5. J. F. Geisz, M. A. Steiner, I. García, S. R. Kurtz and D. J. Friedman, *Applied Physics Letters*, 2013, **103**, 041118.
6. T. Trupke, R. A. Bardos, M. D. Abbott and J. E. Cotter, *Applied Physics Letters*, 2005, **87**, 093503.
7. K. Emery, J. Burdick, Y. Caiyem, D. Dunlavy, H. Field, B. Kroposki, T. Moriarty, L. Ottoson, S. Rummel and T. Strand, *Conference Record of the 25th IEEE PVSC*, 1996.
8. S. Essig, M. A. Steiner, C. Allebé, J. F. Geisz, B. Paviet-Salomon, S. Ward, A. Descoedres, V. LaSalvia, L. Barraud, N. Badel, A. Faes, J. Levrat, M. Despeisse, C. Ballif, P. Stradins and D. L. Young, *IEEE Journal of Photovoltaics*, 2016, **6**, 1012-1019.
9. W. F. Holmgren, C. W. Hansen and M. A. Mikofski, *The Journal of Open Source Software*, 2018, **3**, 884.